Journal of Colloid and Interface Science 571 (2020) 348–355

Contents lists available at ScienceDirect

Journal of Colloid and Interface Science

journal homepage: www.elsevier.com/locate/jcis

Alternating magnetic field mediated release of fluorophores from magnetic nanoparticles by hysteretic heating

Jonathan S. Casey [a], Julien H. Arrizabalaga [a], Mohammad Abu-Laban [b], Jeffrey C. Becca [c], Benjamin J. Rose [a], Kevin T. Strickland [a], Jacob B. Bursavich [d], Jacob S. McCann [e], Carlos N. Pacheco [c,f], Lasse Jensen [c], Anilchandra Attaluri [g], Daniel J. Hayes [a,h,i,*]

[a] The Department of Biomedical Engineering, The Pennsylvania State University, University Park, PA 16802, United States
[b] Feinberg School of Medicine, Northwestern University, Chicago, IL 60611, United States
[c] The Department of Chemistry, The Pennsylvania State University, University Park, PA 16802, United States
[d] The Department of Agricultural and Biological Engineering, Louisiana State University, Baton Rouge, LA 70803, United States
[e] The Department of Biochemistry and Molecular Biology, The Pennsylvania State University, University Park, PA 16802, United States
[f] The NMR Facility, The Pennsylvania State University, University Park, PA 16802, United States
[g] The Department of Mechanical Engineering, The Pennsylvania State University, Harrisburg, PA 17057, United States
[h] Materials Research Institute, Millennium Science Complex, The Pennsylvania State University, University Park, PA 16802, United States
[i] The Huck Institute of the Life Sciences, Millennium Science Complex, The Pennsylvania State University, University Park, PA 16802, United States

GRAPHICAL ABSTRACT

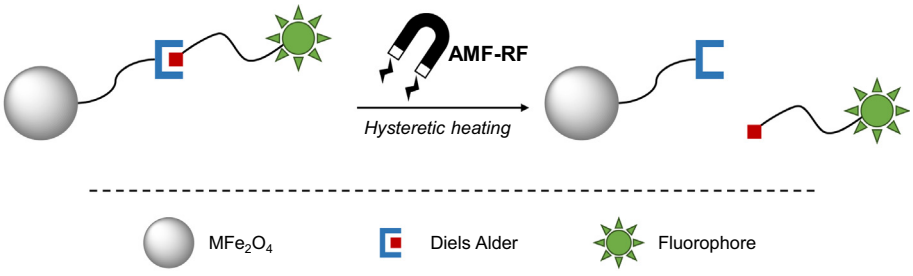

ARTICLE INFO

Article history:
Received 13 November 2019
Revised 24 February 2020
Accepted 16 March 2020
Available online 17 March 2020

Keywords:
Magnetic
Nanoparticles
Diels-Alder
Controlled release
Alternating magnetic field
Iron oxide

ABSTRACT

This study explores the use of differential heating of magnetic nanoparticles with different sizes and compositions (MFe_2O_4 (M = Fe, Co)) for heteroplexed temporal controlled release of conjugated fluorophores from the surface of nanoparticles. By exploiting these differences, we were able to control the amount of hysteretic heating occurring with the distinct sets of magnetic nanoparticles using the same applied alternating magnetic field radio frequency (AMF-RF). Using thermally labile retro-Diels-Alder linkers conjugated to the surface of nanoparticles, the fluorescent payload from the different nanoparticles disengaged when sufficient energy was locally generated during hysteretic heating. 1H, 13C NMR, ESI-MS, and SIMS characterized the thermally responsive fluorescent cycloadducts used in this study; the Diels Alder cycloadducts were modeled using density functional theory (DFT) computations. The localized point heating of the different nanoparticle compositions drove the retro-Diels-Alder reaction at different times resulting in higher release rates of fluorophores from the $CoFe_2O_4$ compared to the Fe_3O_4 nanoparticles.

© 2020 Elsevier Inc. All rights reserved.

* Corresponding author at: The Department of Biomedical Engineering, The Pennsylvania State University, University Park, PA 16802, United States.
E-mail address: djh195@psu.edu (D.J. Hayes).

https://doi.org/10.1016/j.jcis.2020.03.056
0021-9797/© 2020 Elsevier Inc. All rights reserved.

1. Introduction

Improved spatiotemporal control of drug release can address common concerns such as acute toxicity from therapeutics and off target effects of drugs. The characteristics associated with magnetic nanoparticles make these strong candidates for addressing these issues. The ability of magnetic nanoparticles (MNPs) to generate heat locally in response to an alternating magnetic field, its recognized bio-compatibility, and use in clinical practice (i.e. MRI contrast agent), make MNPs appealing candidates for biomedical applications. MNPs have been used for a variety of biomedical applications such as: cancer/gene therapy, hyperthermia, and imaging [1–3]. Several compositions of magnetic nanoparticles are biocompatible and FDA approved [4].

In several magnetic nanoparticle studies, radiofrequency alternating magnetic field has been used for controlled drug delivery [5–7]. Controlled release of encapsulated doxorubicin by remote activation of magnetic nanoparticles using AMF-RF stimulation was reported for the treatment of S180 mice tumors [7]. In another study involving magnetic nanoparticles, the surfaces of MNPs were coated with poly(ethyleneimine) (PEI) and conjugated with the molecule allyl isocyanate (AITC). When rat neurons treated with the modified nanoparticles were stimulated via AMF-RF, the AITC was released. This resulted in the discharge of Ca^{2+} ions, subsequently stimulating neurons [5]. Research involving combinatorial therapy and magnetic nanoparticles has also been reported. The therapeutics doxorubicin and erlotinib, were incorporated into the carbon shells of magnetic iron oxide nanoparticles for controlled drug release [6]. The study examined controlled pH/RF release of therapeutics on PANC-1 cells, as well as the synergistic effects of the drugs when coupled with magnetic hyperthermia. The combinatorial therapy of doxorubicin, erlotinib, and hyperthermia demonstrated increased cell death of pancreatic cancer cells.

In the present study, Diels-Alder cycloadducts are synthesized and conjugated to the surface of magnetic nanoparticles and fluorophores are used as a model for controlled payload release. Different release rates of fluorophores were evaluated using different composition nanoparticles under the same applied AMF-RF conditions and settings. Using $CoFe_2O_4$ and Fe_3O_4 with similar Diels Alder cycloadducts, controlled release of different fluorophores was assessed. This was performed by using differences in hysteric heating from the different composition magnetic nanoparticles in the same solution. It was determined that the release rates of the fluorophores from a combination of different composition magnetic nanoparticles in the same solution correlated to the composition and were similar to the release when particle types were tested individually. In these magnetic nanoparticle delivery systems, the amount of energy input via hysteretic heating, is positively correlated to the payload released using the Diels-Alder cycloadduct with no burst release of the payload. In addition, unlike other systems (i.e. PEI) which have payload release at lower energies ($\leq$40 °C), the Diels-Alder cycloadduct can be tailored to have higher transition energy requirements (>60 °C) which would make delivery of the desired payload more stable and predictable. This demonstration of controlled release of fluorophores from MNPs illustrates the potential of Diels-Alder cleavage for targeted payload release.

2. Materials and methods

2.1. Reagents

Iron (III) chloride hexahydrate (>98%), iron chloride tetrahydrate (>99%), nitric acid (70%), sodium chloride (>99%), sodium bicarbonate (>98%), hydrochloric acid (37%), sodium phosphate dibasic anhydrous, dopamine hydrochloride, anhydrous dimethyl sulfoxide (99.8%), cobalt(II) nitrate hexahydrate (99.9%), ammonium hydroxide (28%), and Alexa Fluor™ 488 C5 Maleimide were purchased from Millipore Sigma. Sodium hydroxide (98%), sodium citrate tri-sodium salt dehydrate, sulfur succinimidyl 4-(*N*-maleimidomethyl) cyclohexane-1-carboxylate, and 5-((2-(and-3)-S-(acetylmercapto) succinoyl) amino) fluorescein (SAMSA) were purchased from Thermofisher Scientific. 2-thiophenemethanethiol (>95%) and N-[4-(2-Benzimidazolyl) phenyl] maleimide (98%) were purchased from TCI America.

2.2. Nanoparticle synthesis

The MFe_2O_4 (M = Fe, Co) was prepared and characterized as in the literature with minor alterations [8,9]. Fe_3O_4 nanoparticles were synthesized using the co-precipitation method. 2.16 g of $FeCl_3{\cdot}6H_2O$ was dissolved in 4 mL of 1 M HCl, and 0.93 g $FeCl_2 \cdot 4H_2O$ was dissolved in 2 mL of 1 M HCl. These solutions were mixed together, and then 54 mL of H_2O was added. The solution was then brought to 95 °C and maintained at this temperature for the rest of the synthesis. Next, 12.5 mL of 28% ammonium hydroxide solution was added to the mixture and stirred for 1 h. The solution was then treated with 1 M H_2NO_4 until the solution attained a pH of 4–7, after which, the mixture was allowed to incubate at room temperature for 24 h. Subsequently, the solution with the nanoparticles was washed 3x with deionized water, and the pH was adjusted to 7 (via washes). The nanoparticles were then magnetically separated. $CoFe_2O_4$ nanoparticles were also synthesized using the co-precipitation method. 0.91 g of $FeCl_3{\cdot}6H_2O$ was added to 6.7 mL of 1 M HCL. 0.49 g $Co(NO)_2{\cdot}6H_2O$ was added to 3.35 mL of 1 M HCl. These two solutions were mixed together, heated to 95 °C and maintained at this temperature for the rest of the synthesis. 4.20 g of NaOH was diluted with 35 mL of H_2O, and added to the mixed solution. The mixed solution was heated and stirred for 1 h. The solution was then treated with 1 M H_2NO_4 until the solution attained a pH of 4–7, the mixture was allowed to sit for 24 h. Subsequently, the solution with the nanoparticles was washed 3x with deionized water, and the pH was adjusted to 7 (via washes). The nanoparticles were magnetically separated.

2.3. Size sorting of $CoFe_2O_4$ and Fe_3O_4

The different composition nanoparticles were size sorted using a method outlined in the literature [10]. Briefly, the different sets of unmodified nanoparticles were heated at 80 °C in an aqueous saturated sodium citrate solution for 30 min. The stable nanoparticles were then treated with a solution of 0.45 M sodium chloride. The precipitate and the suspensions were separated from one another, and the procedure was repeated 3 times, to attain monodisperse nanoparticles. $CoFe_2O_4$ and Fe_3O_4 nanoparticles were characterized using an FEI Tecnai G20 20 XTWIN transmission electron microscope. The X-ray diffraction patterns of these nanoparticles were obtained using a Malvern Panalytical Empyrean (3rd gen.) equipped with a Co source.

2.4. Synthesis of Diels-Alder linker

The Diels-Alder linker was synthesized according to the literature with minor modifications [11]. 1.5 μL of 2-Thiophenemethanethiol and 8.33 mg of Alexa Fluor™ 488 C_5 - Maleimide were dissolved in 10 mL of anhydrous methanol. The pH of the solution was adjusted to 3.5–4 by 0.1 M HCl. The reaction mixture was heated at 60 °C for 3 days. 4.16 μL of 2-Thiophenemethanethiol and 2.71 mg of N-[4-(2-Benzimidazolyl)phenyl]maleimide were dissolved in 10 mL of methanol. The pH of

the solution was adjusted to 3.5–4 by 1 M HCl. The reaction mixture was heated at 60 °C for 3 days.

2.5. Activation of SAMSA fluorescein

The 5-((2-(and-3)-*S*-(acetylmercapto) succinoyl) amino) fluorescein (SAMSA) was used as a control and was activated according to the product instructions (ThermoFisher Scientific; SAMSA Fluorescein; A685). Briefly, 2 mg of SAMSA fluorescein was dissolved in 200 μL of 0.1 M NaOH. The product was incubated at room temperature for 15 min. After, 2.8 μL of 6 M HCl was used to neutralize the solution, followed by 40 μL of 0.5 M sodium phosphate to buffer the solution.

2.6. Computational methods

Calculations for all geometries and frequencies were performed using NWChem 6.8.1 [12] with the B3LYP [13–16] functional and a 6-311G* basis set. Geometry optimizations were performed for the gradient, gradient max, gradient root mean square, Cartesian maximum step and root mean square. Transition state searches were performed with reactant structures initially constrained to 2.4 Å for the reacting carbon atoms. The zero point energies and other thermodynamic data were obtained from the numerical frequency calculations performed with extra fine grid settings at 25, 40, 60, and 80 in degree Celsius. All calculations were performed as gas phase with no solvent effects.

2.7. Nanoparticle modification with Diels Alder cycloadducts

In previous studies, different retro-Diels-Alder cycloadducts have been conjugated to gold or silver nanoparticles [11,17]. Nanoparticles were modified in a series of sequential steps consisting of the addition of: dopamine HCl, sulfo-SMCC, and retro-Diels Alder linker. The attachment scheme is reported in Fig. 1. The nanoparticle modification with dopamine HCl occurred as stated in the literature with minor changes [18]. 10 mg of nanoparticles and excess dopamine HCl were dissolved in methanol. The solution was sonicated for 1 h. The nanoparticles were magnetically separated, and the supernatant was removed. The nanoparticles were washed 1x with saturated sodium bicarbonate solution and magnetically decanted. The nanoparticles were subsequently washed 2x with 70%EtOH/30%H_2O, and magnetically separated. After the washes, the modified nanoparticles were put in a solution of 70% EtOH/30%H_2O. To link the amine with the thiolated cycloadduct, the sulfo-SMCC linker was added using the stated protocol (ThermoFisher Scientific 22322). For conjugation of the terminal amine to the sulfo-SMCC, the pH was adjusted to 7–7.5 pH using 1 M NaOH and 1 M HCl solutions. For 1 mg of modified nanoparticles, 100 μL of 10 mg/mL of sulfo-SMCC dissolved in dimethyl sulfoxide (DMSO) was added. The reaction was placed on a rocker for 4 h. After modification, the suspension was washed 2x with 70% EtOH/30% H_2O and 1x with anhydrous MeOH. The supernatant was removed, and the pellet was resuspended in retro-Diels-Alder solution. The pH of the solution was adjusted using 0.1 M NaOH and 0.1 M HCl solutions. The pH was adjusted to be 6.5.

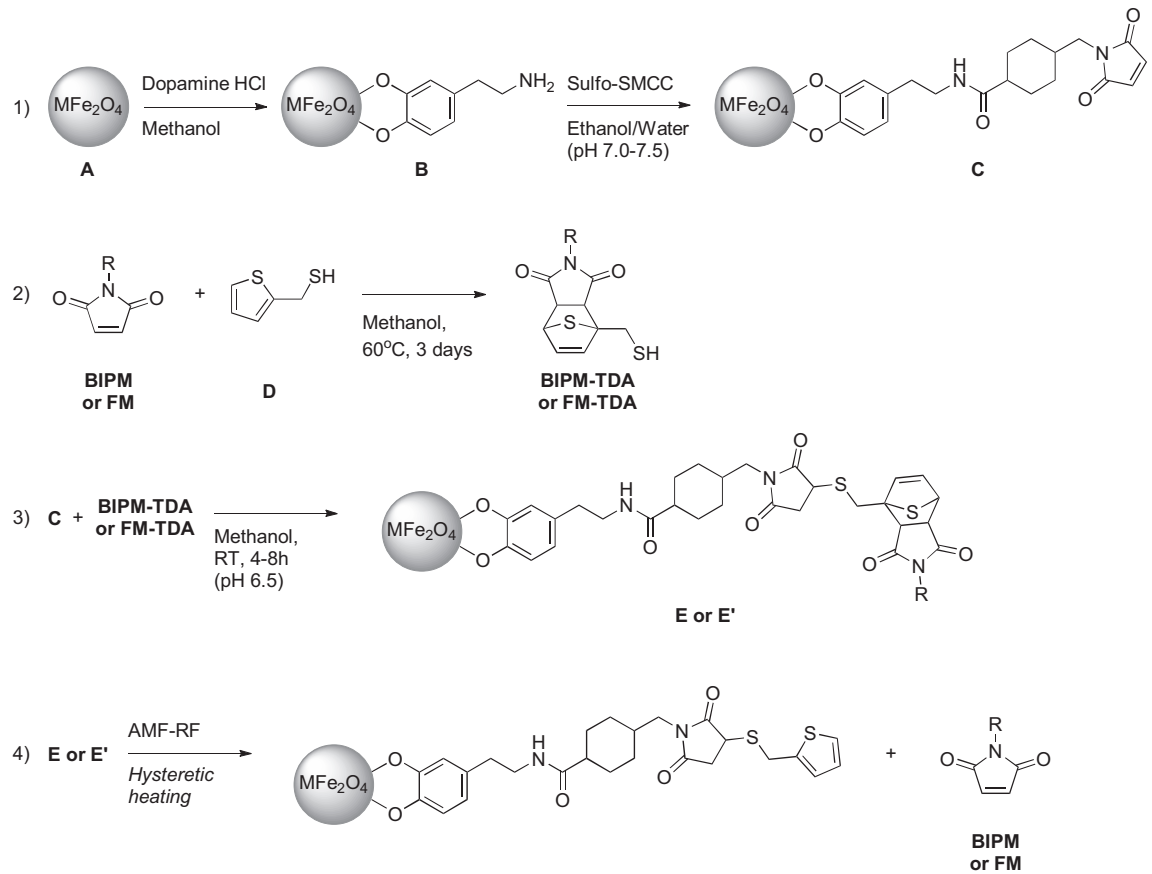

Fig. 1. Attachment Scheme for MFe_2O_4 (M = Fe, Co) nanoparticles. (1) Conjugation of Dopamine HCl and Sulfo-SMCC. (2) Preparation of Thiophenemethanethiol based Diels Alder linkers with maleimide conjugated fluorophores. (3) Conjugation of Diels-Alder linkers to previously modified nanoparticles. (4) Retro Diels-Alder reaction triggered by the AMF-RF hysteretic heating.

The solution was mixed with the modified nanoparticles for 4–8 h at room temperature. After the elapsed time, the sample was washed and magnetically separated. The sample was washed 3x with anhydrous MeOH, and suspended in anhydrous DMSO.

2.8. AMF-RF hysteretic heating of Fe_3O_4 and $CoFe_2O_4$

The equipment used for the AMF-RF hysteretic heating was a Nanotherics magneTherm^{Tm} Limited. The AMF-RF coil used was a 17-turn coil with a 50 mm diameter, the radiofrequency was 626.8 kHz, the DC power supply voltage 31 V and the DC power supply current 7.5A. This inductive heating device had an adequate quasi-adiabatic isolation due to a connection to a recirculating water chiller maintaining the coil temperature at a constant 15 °C throughout the operation of the device. The sample was thermally isolated by a Styrofoam holder while inserted into the coil and therefore the sample only heated up from stimulation from the alternating magnetic field. For AMF-RF hysteretic heating, $CoFe_2O_4$ and Fe_3O_4 nanoparticles were stabilized in H_2O. The temperatures readings were measured with a Lascar EL-USB-TC-LCD USB Thermocouple Logger with a LCD Display. The thermocouple used was type T. Heating magnetic ferro-fluids by using an alternating magnetic field and calculating corresponding SLP values has previously been described in the literature [19]. For SLP measurements, each sample was stabilized in a 1.5 mL Eppendorf tube with 1 mL of water. The tube was closed and placed in a Styrofoam insulated receptacle, heated for 60 s, and the temperature measured using a thermocouple probe. The temperature was recorded every second for 60 s. The number of samples used for each set of nanoparticles was n = 3.

2.9. Determining the alternating magnetic field strength

A commercially available radiofrequency magnetic field probe (AMF Life Systems, Auburn Hills, MI) was used to determine the magnetic field strength output of the coil. Briefly, the tip of the probe was inserted in the same position as the nanoparticles for heating and an oscilloscope was used to measure the AC voltage difference generated at the ends of the probe. The magnetic flux density was measured for both the axial and radial direction. More details about the calculation of the magnetic field strength are provided in the Supporting Material.

2.10. AMF-RF hysteretic heating of modified Fe_3O_4 and $CoFe_2O_4$

The modified nanoparticles underwent AMF-RF stimulation in 1 mL of anhydrous dimethyl sulfoxide. After modification and purification of $CoFe_2O_4$ and Fe_3O_4 NPs (i.e. conjugated with fluorescein maleimide Diels Alder cycloadduct and BIPM Diels Alder cycloadduct), the modified nanoparticle solution was placed into a 1.5 mL plastic (up to a volume of 1 mL) Eppendorf tube. The concentrations for the individual samples were 0.068 mg/mL for iron oxide nanoparticles and 0.058 mg/mL for cobalt iron oxide, as confirmed by ICP-OES. When the nanoparticles were put together for heated release, the concentration of modified iron oxide was 0.068 mg/mL and modified cobalt iron oxide was 0.058 mg/mL for a total concentration of 0.063 mg/mL. Time points for the hysteretic heating of the individually modified $CoFe_2O_4$ and Fe_3O_4 samples were recorded every 3 min up to 24 min. Time points for the hysteretic heating of the combined modified $CoFe_2O_4$ and Fe_3O_4 occurred every 5 min up to 20 min. The number of sample run for each set of nanoparticles was n = 3. After hysteretic heating, the samples were magnetically separated. In addition, the supernatant was spun down at 80 k rpms for two hours to ensure all of the magnetic nanoparticles were separated from the solution. The centrifuge used was an Optima^{TM} TLX Ultracentrifuge 120 k and the centrifuge tubes used were polypropylene. In order to detect UV-fluorescence from the BIPM, the samples were derivatized with 10 μL of 2-mercaptoethanol and measured in a quartz cuvette. After this reading, the sample was treated with 0.5 mL of PBS (-) and the fluorescein's intensity was measured. Every sample was treated with the same amount of 2-mercaptoethanol and PBS (-). This was done to determine the fluorophore's intensity. BIPM fluorescence measurement excitation was 315 nm and its emission was 365 nm post-derivitization. The fluorescein maleimide measurement after being treated with PBS (-) was 494 nm excitation and 512 nm emission. The measurements were taken with a Spectra M5 Microplate/Cuvette Reader (Molecular Devices, PA, USA).

2.11. AMF-RF hysteretic heating of modified $CoFe_2O_4$ with conjugated SAMSA

A negative control to the experiment was setup to ensure the Diels Alder linker was cleaved during AMF-RF stimulation, and not breakage of another bond in the conjugated nanoparticle structure. The SAMSA fluorophore was directly conjugated to the $CoFe_2O_4$ (due to a higher SLP value), similarly to the Diels Alder cycloadducts (Supporting Material Figs. S5, S6, and S7). In these experiments, the modified nanoparticles underwent AMF-RF stimulation in anhydrous dimethyl sulfoxide. After modification and cleanup of SAMSA $CoFe_2O_4$, the modified nanoparticle solution was placed in a 1.5 mL plastic (up to a volume of 1 mL) Eppendorf tube. The individual samples were heated at 0.1 mg/mL for cobalt iron oxide concentration modified nanoparticles (confirmed by ICP-OES), before undergoing hysteretic heating via AMF-RF stimulation. The hysteretic heating of the modified SAMSA $CoFe_2O_4$ occured at 5-minute intervals up to 20 min. The number of sample run for each set of nanoparticles was n = 3. After hysteretic heating, the samples were magnetically decanted. In addition, the supernatant was spun down at 80 k rpms for two hours to ensure all the magnetic nanoparticles were separated from the solution. The centrifuge used was an Optima^{TM} TLX Ultracentrifuge 120 k and the centrifuge tubes used were polypropylene (Beckman Coulter Ref # 347287). The sample was then treated with 0.5 mL of PBS (-) and fluorescent intensity was measured. For the samples, the groups were normalized to the fluorescent intensity on the 0 min time point. The fluorescein maleimide measurement was 494 nm excitation and 512 nm emission. The different group supernatants showed a fluorescence of (mean ± STD) 2.73 ± 0.30 percent release up to 20 min. The measurements were taken in a quartz cuvette with a Spectra M5 Microplate/Cuvette Reader.

2.12. ICP-OES analysis

Ion coupled plasma optical emission spectroscopy (ICP-OES) was performed on the individual samples to determine the Fe_3O_4 and $CoFe_2O_4$ concentrations. This technique has previously been reported to determine the content of cobalt and iron in nanoparticles [20,21]. The samples were in 1 mL of H_2O and analyzed using a Perkin Elmer Optima 5300 ICP-OES instrument. 500 μL of sample was dissolved with 500 μL of concentrated nitric acid, and then diluted with 9 mL of DI water to a final volume of 10 mL. The iron content determined by ICP-OES was 0.789 ± 0.062 mg and the cobalt iron content was 0.197 ± 0.007 mg. The analysis was conducted in triplicate.

2.13. Immersion heating of Diels-Alder fluorophores

In order to assess the total amount of fluorophore conjugated to the nanoparticles, samples of different sets of modified nanoparticles in anhydrous DMSO were placed in a hot oil bath (inside a

plastic Eppendorf tube) for 3 h and heated at 80 °C to induce the retro Diels-Alder reaction and the fluorophore release in solution. This is similar to what has been performed to analogous thiophene Diels-Alder cycloadducts conjugated to nanoparticles in the literature [22]. Release of the BIPM fluorophore was quantified by measuring BIPM maleimide at 315 nm (365 nm excitation) after being derivatized with 10 μL of 2-mercaptoethanol. Release of fluorescein maleimide was quantified by measuring the fluorescence at 494 nm (518 nm excitation). The measurements were taken with a Spectra M5 Microplate/Cuvette Reader.

2.14. Secondary Ion mass Spectrometry analysis

SIMS analysis [20,23,24] was performed to attain information on the fluorophore conjugation to the nanoparticles. Each sample was dried out into a powder form, applied to a stage, and analyzed by SIMS. The analysis was performed in positive mode at 70 keV $(CO_2)^+_{15,000}$. The instrument used for the analysis was a Lonoptika J105 3D Chemical Imager similar to other studies [25].

2.15. Statistical analysis

A two-way analysis of variance (ANOVA) was performed on the time points for the different sets of nanoparticles to determine if a statistical difference existed between the two groups regarding the release of fluorophores. For each of the analysis a confidence interval of 95% was used and the number of samples was n = 3. The software GraphPad Prism 6.01 was used for statistical analysis.

3. Results and discussion

Density functional theory calculations were performed on the Diels-Alder cycloadducts. This was done to determine the forward and reverse reaction energies for the different linkers as well as their endo vs exo products. This was performed to determine the specific energies at which the reactions would go forward, and if there were different cleavage rates for the linkers and their endo vs exo products. Fig. 2 shows the structures of the Diels-Alder products which were simulated using B3LYP/6-311G*.

In Table 1, the enthalpy barriers and Gibbs free energy are displayed for both cycloadducts as well as their respective endo and exo products. These models indicate that each of the respective retro-Diels-Alder cycloadducts have comparable reverse reaction energies. The respective endo and exo products of each linker are also close in the energy required to drive the retro-Diels-Alder reaction, indicating that both species will have a similar release rate of the fluorophores during hysteretic heating as opposed to the release of the endo and the exo product at separate times. Table 1 includes the values for the products of the forward and reverse reactions.

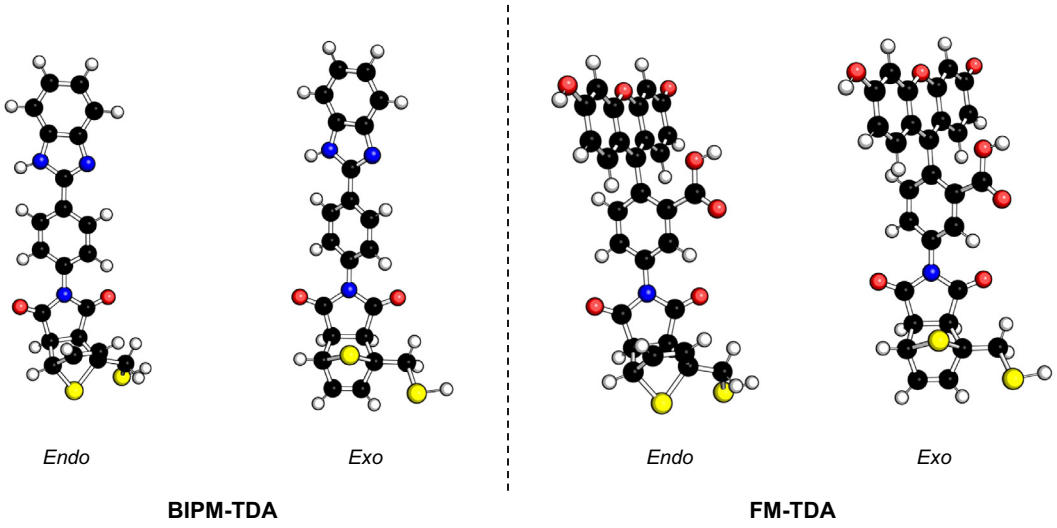

Fig. 2. Structures of endo and exo products for both BIPM-TDA and FM-TDA were obtained using NWChem 6.8.1 [12] with the B3LYP and 6-311G* computational set [14–16,26]. Yellow Atoms: Sulfur; Black Atoms: Carbon; White Atoms: Hydrogen; Red Atoms: Oxygen. Images were created using the PyMOL molecular graphics system. Transition states for these molecules are reported in the Supporting Material Fig. S1. (For interpretation of the references to colour in this figure legend, the reader is referred to the web version of this article.)

Table 1
Gibbs Free Energy and Enthalpy simulated barrier heights of forward and reverse reactions for BIPM-TDA and FM-TDA cycloadducts. Values were generated with the B3LYP [14–16,26] functional and a 6-311G* basis set.

		Reaction Barriers for ΔH_{rxn} (kcal/mol)				Reaction Barriers for ΔG (kcal/mol)			
Diels-Alder product	T (°C) Reaction	25	40	60	80	25	40	60	80
BIPM-TDA Endo	Forward	29.98	29.99	30.00	30.02	44.36	45.08	46.05	47.01
	Reverse	28.24	28.25	28.27	28.29	26.82	26.74	26.65	26.55
BIPM-TDA Exo	Forward	29.86	29.87	29.89	29.91	44.37	45.10	46.07	47.04
	Reverse	27.72	27.74	27.76	27.78	26.69	26.64	26.57	26.49
FM-TDA Endo	Forward	29.47	29.48	29.50	29.52	43.82	44.54	45.50	46.46
	Reverse	27.84	27.85	27.88	27.89	26.39	26.32	26.22	26.12
FM-TDA Exo	Forward	29.38	29.39	29.41	29.43	43.96	44.70	45.68	46.65
	Reverse	27.35	27.37	27.39	27.40	26.33	26.28	26.21	26.14

The different composition Fe_3O_4 and $CoFe_2O_4$ nanoparticles were analyzed via powder X-ray diffraction. Fig. 3 shows the XRD pattern of $CoFe_2O_4$ and Fe_3O_4 nanoparticles respectively. The XRD patterns show a similar peak distribution with the different nanoparticle compositions as seen with the peaks and its corresponding Miller Indices. The crystallinity of the distinct composition nanoparticles (inverse spinel structure), allowed for a conserved attachment chemistry to be utilized for the different composition nanoparticles. Reported in the literature, different spinel ferrites (MFe_2O_4 with M = Co, Ni, Mn, or Fe) with an established synthesis, show similar XRD patterns [27]. A Rietveld refinement was performed on each set of nanoparticles. The refinement revealed a size distribution of 7.9 ± 0.2 nm in diameter for Fe_3O_4 nanoparticles and a size distribution of 12.1 ± 0.1 nm in diameter for $CoFe_2O_4$ nanoparticles.

Magnetic hysteresis tests were performed on both Fe_3O_4 and $CoFe_2O_4$ nanoparticles. In Fig. 4, the magnetization for the $CoFe_2O_4$ nanoparticles is higher than the one for the Fe_3O_4 nanoparticles. Given the SLP values obtained for the different magnetic nanoparticles (Fig. 5), the hysteresis curves for the two compositions nanoparticles correspond to an expected trend.

In order to demonstrate sequential release from the different composition nanoparticles, AMF-RF conditions were assessed. The magnetic field amplitude was measured using a Hall effect sensor probe (details about these calculations are provided in the Supporting Material). The specific loss power (SLP) values were evaluated using a radiofrequency of 626.8 kHz and a magnetic field strength H_o of 20.0 kA m^{-1}. The Fe_3O_4 nanoparticles used in this study were 7.9 ± 0.2 nm in diameter, and the $CoFe_2O_4$ nanoparticles were 12.1 ± 0.1 nm in diameter. The SLP values calculated for Fe_3O_4 and $CoFe_2O_4$ nanoparticles were 78 and 355 W g^{-1} respectively (Fig. 5). These values are comparable to the ones previously reported in the literature for similar nanoparticles and AMF-RF systems [2,28,29].

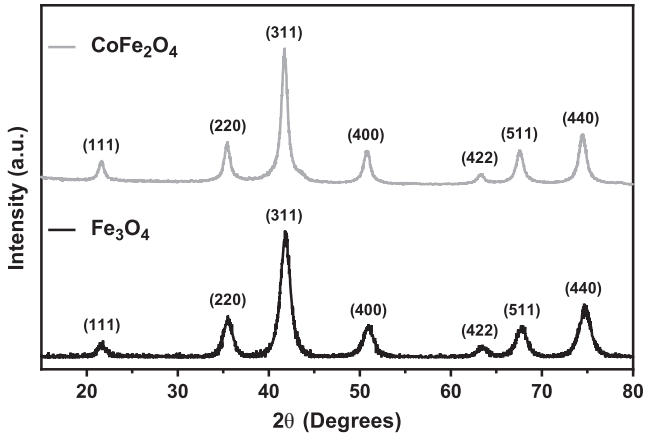

Fig. 3. X-ray diffraction patterns for $CoFe_2O_4$ (in grey) and Fe_3O_4 (in black) nanoparticles.

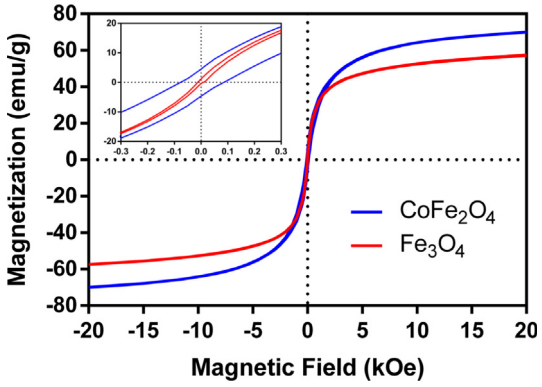

Fig. 4. Magnetic hysteresis curves for $CoFe_2O_4$ and Fe_3O_4 nanoparticles. The inset panel contains a zoom on the area of small magnetic fields.

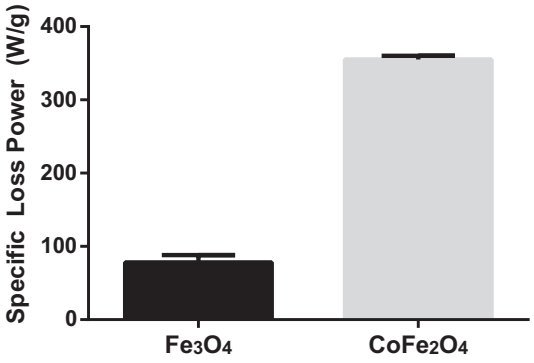

Fig. 5. Specific Loss Power values for the Fe_3O_4 and $CoFe_2O_4$ nanoparticles at a radio frequency of 626.80 kHz and a magnetic field strength of 20.0 kA m^{-1}.

In order to confirm successful modification of the different composition nanoparticles, Secondary Ion Mass Spectrometry (SIMS) was performed on the modified Fe_3O_4 and $CoFe_2O_4$ nanoparticles and products with the expected mass of each Diels-Alder linker and fluorophore were found on the nanoparticles indicating successful conjugation (Supporting Material Figs. S3 and S4).

Fluorescent release was measured for different sets of nanoparticles with the thiophene based Diels-Alder linkers. In Fig. 6, release of fluorescein maleimide from the modified $CoFe_2O_4$ and release of BIPM (post-derivatized) from the modified Fe_3O_4 is shown.

A significantly higher release rate of fluorophore was seen with the cobalt iron oxide vs iron oxide nanoparticles at each time point, which correlates with the $CoFe_2O_4$ nanoparticles having a SLP value higher than the Fe_3O_4 nanoparticles.

To demonstrate sequential and controlled release, the different composition modified nanoparticles were mixed in suspension together and underwent hysteretic heating using AMF-RF stimulation (Fig. 7). The fluorophore conjugated to the $CoFe_2O_4$ nanoparticles released before the one conjugated to the Fe_3O_4 nanoparticles as predicted by the individual release profiles reported in Fig. 6.

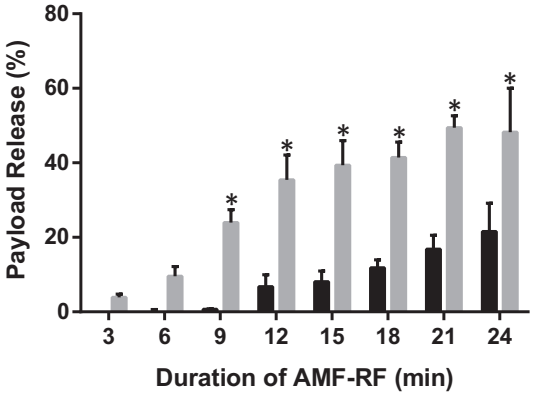

Fig. 6. Payload release from $CoFe_2O_4$ nanoparticles conjugated with FM-TDA linker (in grey), and Fe_3O_4 nanoparticles conjugated with BIPM-TDA (in black). *Significant differences ($p < 0.05$) when compared to the Fe_3O_4 nanoparticles group at the same time point.

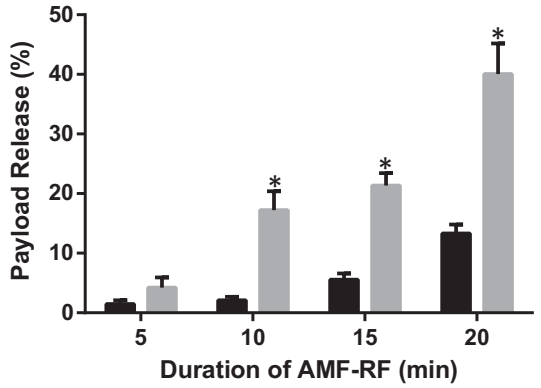

Fig. 7. Sequential payload release from $CoFe_2O_4$ nanoparticles conjugated with FM-TDA linker (in grey), and Fe_3O_4 nanoparticles conjugated with BIPM-TDA (in black) when both particle sets are combined in solution. *Significant differences ($p < 0.05$) when compared to the Fe_3O_4 nanoparticles group at the same time point.

The payload release rates between the two different nanoparticles were statistically significant at the 10, 15 and 20 min time points.

In addition to the release studies using Diels Alder cycloadducts, a control study was performed using a similar conjugation chemistry to verify that the payload release was triggered by the retro Diels-Alder reaction under AMF-RF stimulation. In place of the Diels Alder cycloadducts, the SAMSA fluorophore with an activated thiol was conjugated to $CoFe_2O_4$ nanoparticles via the Sulfo-SMCC linker (Supporting Material Figs. S5 and S6). Samples were prepared at a nanoparticle concentration of 0.1 mg/mL, submitted to AMF-RF hysteretic heating, and the supernatant fluorescence was measured at the 0, 5, 10, 15 and 20 min time points (Supporting Material Fig. S7). Less than 2% of the fluorescent payload was released for all the time points, showing the stability of the first two attachment steps on nanoparticles as illustrated in Fig. 1.

Hysteretic heat dissipation from magnetic nanoparticles MFe_2O_4 (M = Fe, Co) using alternating magnetic field radio frequency (AMF-RF) has been theoretically and experimentally investigated [28]. The SLP values for different nanoparticle compositions can be attributed to the size, shape, and composition of the different nanoparticles[2]. A difference in composition nanoparticles and SLP values for different size (i.e. 7.9 nm in diameter for the Fe_3O_4 nanoparticles and 12.1 nm for the $CoFe_2O_4$) were evaluated in this study. For future biological applications, hysteretic heating using parameters with alternating magnetic fields <20 kA m^{-1} and radio frequencies <1 MHz would need to be met [28,30]. The coil and particular heating parameters chosen for this study resulted in a rapid point heating of the nanoparticles (Supporting Material Fig. S8), triggering the retro Diels-Alder cycloadduct cleavage, and the release of the fluorophore payload. Having a predictive and experimental model of SLP values for nanoparticles, allows the experimenter to tailor NP systems for specific applications.

Different composition ferrite nanoparticles have been shown in the literature to have similar crystallinity [27]. The similar crystal structure for the different composition nanoparticles allowed for a conserved attachment chemistry. This allowed for a chemical modification and attachment technique to be broadly applied to MFe_2O_4 (M = Fe, Co, Mn) nanoparticles, which can be similarly modified. This, while providing different hysteretic heating profiles which can be tailored to create a payload delivery system matched to a specific application.

In this study, a Diels Alder thiophene cycloadduct was used, and sequential release of fluorophores was observed. Given the results, this delivery system could be utilized for multiplexed spatiotemporally controlled payload delivery using different nanoparticle compositions and specific AMF-RF conditions to control payload release rates. An effective way of utilizing this easy to make delivery system, would be to put the primary payload onto the $CoFe_2O_4$ nanoparticles, and the secondary payload onto the Fe_3O_4 nanoparticles. The sequential release would occur by AMF-RF stimulation of the different nanoparticle composition using the same Diels-Alder linkers.

4. Conclusion

The results of the study demonstrate a controlled and predictable release of fluorophores from the surface of different composition magnetic nanoparticles. The $CoFe_2O_4$ NPs with its conjugated fluorescein Diels-Alder cycloadduct had a more rapid release during hysteretic heating compared to the Fe_3O_4 NPs with its conjugated BIPM Diels-Alder cycloadduct. The differences in release of the fluorophores can be attributed to the difference in heating of the different composition nanoparticles. Given the release profiles of the different fluorophores, analogous retro-Diels-Alder cycloadducts can be used as tools for sequential payload release. Using different composition (or size) nanoparticles can create a range of release for a given time under AMF-RF stimulation. The proposed delivery system advantages include ease of use and spatiotemporal release of the desired payload over targeted areas. The system provides an effective way of attaching different payloads to the surface of nanoparticles, with predictable release at desired times by AMF-RF stimulation.

CRediT authorship contribution statement

Jonathan S. Casey: Conceptualization, Methodology, Validation, Formal analysis, Investigation, Writing - original draft, Writing - review & editing, Visualization. **Julien H. Arrizabalaga:** Conceptualization, Formal analysis, Investigation, Writing - review & editing, Visualization. **Mohammad Abu-Laban:** Conceptualization, Methodology, Investigation. **Jeffrey C. Becca:** Methodology, Software, Investigation, Data curation. **Benjamin J. Rose:** Investigation. **Kevin T. Strickland:** Investigation. **Jacob B. Bursavich:** Investigation. **Jacob S. McCann:** Investigation. **Carlos N. Pacheco:** Formal analysis, Investigation. **Lasse Jessen:** Investigation, Resources, Funding acquisition. **Anilchandra Attaluri:** Methodology, Investigation, Resources, Writing - original draft, Writing - review & editing, Funding acquisition. **Daniel J. Hayes:** Formal analysis, Investigation, Resources, Writing - original draft, Writing - review & editing, Visualization, Supervision, Project administration, Funding acquisition.

Declaration of Competing Interest

The authors declare that they have no known competing financial interests or personal relationships that could have appeared to influence the work reported in this paper.

Acknowledgements

This work was supported by the Office of the Assistant Secretary of Defense for Health Affairs through the Peer Reviewed Medical Research Program under Award No. W81XWH-18-1-0115. Opinions, interpretations, conclusions and recommendations are those of the author and are not necessarily endorsed by the Department of Defense. Dr. Hayes, Dr. Laban and Jonathan Casey acknowledge support from the National Institute of Dental and Craniofacial Research of the National Institutes of Health under award number RDE024790A. Dr. Lasse Jessen and Jeffrey Becca acknowledge support from NSF Award Nos. CHE-1362825 and NRT-1449785. The authors of this study are grateful to Dr. Alfonso Davila for consul-

tation regarding the linkage chemistry to the nanoparticles; Jennifer Grey for assistance with TEM imaging. The authors would like to thank Dr. Tatiana Laremore and Dr. Hua Tian for their assistance with mass spectrometry analysis, Laura Linney for ICP-OES analysis, and Ryan Hoff for assisting with the nanoparticle synthesis. The authors would like to thank Nichole Wonderling and Gino Tambourine for their assistance with powder X-ray diffraction.

Appendix A. Supplementary data

Supplementary data to this article can be found online at https://doi.org/10.1016/j.jcis.2020.03.056.

References

[1] N.S. Gandhi, R.K. Tekade, M.B. Chougule, Nanocarrier mediated delivery of siRNA/miRNA in combination with chemotherapeutic agents for cancer therapy: current progress and advances, J. Control. Release 194 (2014) 238–256.
[2] J.-H. Lee, J.-T. Jang, J.-S. Choi, S.H. Moon, S.-H. Noh, J.-W. Kim, J.-G. Kim, I.-S. Kim, K.I. Park, J. Cheon, Exchange-coupled magnetic nanoparticles for efficient heat induction, Nat. Nanotechnol. 6 (2011) 418.
[3] M. Tan, Y. Wang, X. Song, Y. Wu, Nanomaterials as therapeutic/imaging agent delivery vehicles for tumor targeting theranostics, in: Nanomaterials for Tumor Targeting Theranostics, 2016, pp. 1–42.
[4] D. Bobo, K.J. Robinson, J. Islam, K.J. Thurecht, S.R.J.P.R. Corrie, Nanoparticle-based medicines: A review of FDA-approved materials and clinical trials to date, Pharm. Res. 33 (10) (2016) 2373–2387.
[5] G. Romero, M.G. Christiansen, L. Stocche Barbosa, F. Garcia, P. Anikeeva, Localized excitation of neural activity via rapid magnetothermal drug release, 26 (35) (2016) 6471–6478.
[6] Y. Xu, A. Karmakar, W.E. Heberlein, T. Mustafa, A.R. Biris, A.S. Biris, Multifunctional magnetic nanoparticles for synergistic enhancement of cancer treatment by combinatorial radio frequency thermolysis and drug delivery, Adv. Healthcare Mater. 1 (4) (2012) 493–501.
[7] L. Wang, P. Zhang, J. Shi, Y. Hao, D. Meng, Y. Zhao, Y. Yanyan, D. Li, J. Chang, Z. Zhang, Radiofrequency-triggered tumor-targeting delivery system for theranostics application, ACS Appl. Mater. Interfaces 7 (10) (2015) 5736–5747.
[8] T.T.T. N'Guyen, H.T.T. Duong, J. Basuki, V. Montembault, S. Pascual, C. Guibert, J. Fresnais, C. Boyer, M.R. Whittaker, T.P. Davis, L. Fontaine, Functional iron oxide magnetic nanoparticles with hyperthermia-induced drug release ability by using a combination of orthogonal click reactions, Angew. Chem. Int. Ed. 52 (52) (2013) 14152–14156.
[9] F. Augusto Tourinho, R. Franck, R. Massart, Aqueous ferrofluids based on manganese and cobalt ferrites, J. Mater. Sci. 25 (1990) 3249–3254.
[10] J.-P. Fortin, C. Wilhelm, J. Servais, C. Ménager, J.-C. Bacri, F. Gazeau, Size-sorted anionic iron oxide nanomagnets as colloidal mediators for magnetic hyperthermia, J. Am. Chem. Soc. 129 (9) (2007) 2628–2635.
[11] M. Abu-Laban, R.R. Kumal, J. Casey, J. Becca, D. LaMaster, C.N. Pacheco, D.G. Sykes, L. Jensen, L.H. Haber, D.J. Hayes, Comparison of thermally actuated retro-diels-alder release groups for nanoparticle based nucleic acid delivery, J. Colloid Interface Sci. 526 (2018) 312–321.
[12] M. Valiev, E.J. Bylaska, N. Govind, K. Kowalski, T.P. Straatsma, H.J.J. Van Dam, D. Wang, J. Nieplocha, E. Apra, T.L. Windus, W.A. de Jong, NWChem: A comprehensive and scalable open-source solution for large scale molecular simulations, Comput. Phys. Commun. 181 (9) (2010) 1477–1489.
[13] A.D. Becke, Density-functional thermochemistry. III. The role of exact exchange, J. Chem. Phys. 98 (7) (1993) 5648–5652.
[14] C. Lee, W. Yang, R.G. Parr, Development of the Colle-Salvetti correlation-energy formula into a functional of the electron density, Phys. Rev. B 37 (2) (1988) 785–789.
[15] S.H. Vosko, L. Wilk, M. Nusair, Accurate spin-dependent electron liquid correlation energies for local spin density calculations: A critical analysis, Can. J. Phys. 58 (8) (1980) 1200–1211.
[16] P.J. Stephens, F.J. Devlin, C.F. Chabalowski, M.J. Frisch, Ab initio calculation of vibrational absorption and circular dichroism spectra using density functional force fields, J. Phys. Chem. 98 (45) (1994) 11623–11627.
[17] A.B.S. Bakhtiari, D. Hsiao, G. Jin, B.D. Gates, N.R. Branda, An efficient method based on the photothermal effect for the release of molecules from metal nanoparticle surfaces, 48 (23) (2009) 4166–4169.
[18] M.D. Shultz, J.U. Reveles, S.N. Khanna, E.E. Carpenter, Reactive nature of dopamine as a surface functionalization agent in iron oxide nanoparticles, J. Am. Chem. Soc. 129 (9) (2007) 2482–2487.
[19] R.E. Rosensweig, Heating magnetic fluid with alternating magnetic field, J. Magn. Magn. Mater. 252 (2002) 370–374.
[20] C. Xu, J. Xie, D. Ho, C. Wang, N. Kohler, E.G. Walsh, J.R. Morgan, Y.E. Chin, S. Sun, Au–Fe_3O_4 dumbbell nanoparticles as dual-functional probes, Angewandte Chemie Int. Ed. 47 (1) (2008) 173–176.
[21] R. Tabit, O. Amadine, Y. Essamlali, K. Dânoun, A. Rhihil, M. Zahouily, Magnetic $CoFe_2O_4$ nanoparticles supported on graphene oxide ($CoFe_2O_4$/GO) with high catalytic activity for peroxymonosulfate activation and degradation of rhodamine B, RSC Adv. 8 (3) (2018) 1351–1360.
[22] M. Abu-Laban, R.R. Kumal, J. Casey, J. Becca, D. LaMaster, C.N. Pacheco, D.G. Sykes, L. Jensen, L.H. Haber, D.J. Hayes, Comparison of thermally actuated retro-Diels-Alder release groups for nanoparticle based nucleic acid delivery, J. Colloid Interface Sci. 526 (2018) 312–321.
[23] C. Xu, B. Wang, S. Sun, Dumbbell-like Au−Fe_3O_4 nanoparticles for target-specific platin delivery, J. Am. Chem. Soc. 131 (12) (2009) 4216–4217.
[24] C. Xu, K. Xu, H. Gu, R. Zheng, H. Liu, X. Zhang, Z. Guo, B. Xu, Dopamine as A robust anchor to immobilize functional molecules on the iron oxide shell of magnetic nanoparticles, J. Am. Chem. Soc. 126 (32) (2004) 9938–9939.
[25] J.S. Fletcher, S. Rabbani, A. Henderson, P. Blenkinsopp, S.P. Thompson, N.P. Lockyer, J.C. Vickerman, A new dynamic in mass spectral imaging of single biological cells, Anal. Chem. 80 (23) (2008) 9058–9064.
[26] A.D. Becke, Density-functional thermochemistry. III. The role of exact exchange, 98 (7) (1993) 5648–5652.
[27] N. Bao, L. Shen, Y. Wang, P. Padhan, A. Gupta, A facile thermolysis route to monodisperse ferrite nanocrystals, J. Am. Chem. Soc. 129 (41) (2007) 12374–12375.
[28] R. Chen, M.G. Christiansen, P. Anikeeva, Maximizing hysteretic losses in magnetic ferrite nanoparticles via model-driven synthesis and materials optimization, ACS Nano 7 (10) (2013) 8990–9000.
[29] A.G. Kolhatkar, A.C. Jamison, D. Litvinov, R.C. Willson, T.R. Lee, Tuning the magnetic properties of nanoparticles, Int. J. Mol. Sci. 14 (8) (2013) 15977–16009.
[30] R. Hergt, S. Dutz, Magnetic particle hyperthermia—biophysical limitations of a visionary tumour therapy, J. Magn. Magn. Mater. 311 (1) (2007) 187–192.